Infrared lines as probes of solar magnetic features

V. The magnetic structure of a simple sunspot and its canopy

S.K. Solanki[1], I. Rüedi[1], and W. Livingston[2]

[1] Institute of Astronomy, ETH-Zentrum, CH-8092 Zürich, Switzerland
[2] National Solar Observatory, NOAO*, P.O.Box 26732, Tucson AZ 85726, USA

Abstract. The strength and inclination of the magnetic field of a simple, relatively symmetric sunspot are determined using the extremely Zeeman sensitive Landé $g = 3$ Fe I line at 15648 Å. This spectral line allows a reliable determination of the field strength from the umbra to the outer boundary of the penumbra. The largest field strength observed in the sunspot is approximately 3100 G, the field strength at different points along the outer penumbral edge varies between 800 G and 1000 G. The angle of inclination at the outer penumbral boundary is close to 80°. Using λ 15648 Å, the magnetic field of the sunspot can be followed well beyond the outer edge of the penumbra. A low-lying, almost horizontal superpenumbral magnetic canopy reproduces these observations best, in agreement with the results of Giovanelli & Jones (1982). The magnetic field strength in the canopy can be measured and is found to be consistent with a magnetic monopole. The smallest measured field strength is 300–400 G. Evidence of small magnetic elements underlying the superpenumbral canopy is presented. The return-flux model of sunspot magnetic fields (Osherovich 1982, Flå et al. 1982) is not compatible with the present observations. They also do not support a lower boundary of the penumbral magnetic field that lies significantly above the continuum formation level, or the presence of field-free gas in more than 10% of the penumbral volume in the lower photosphere.

Key words: the Sun: magnetic fields – sunspots – infrared radiation – polarimetry

1. Introduction

Sunspots are the solar magnetic features most easily accessible to direct observations and have invited considerable attention. Nevertheless, much of their physics remains unresolved (see the proceedings edited by Cram & Thomas 1981 and by Thomas & Weiss 1992, as well as the review by Moore & Rabin 1985). Although many of the open questions are related to the magnetic or thermal fine structure, a number of global aspects of sunspot magnetic fields are also unclear.

We address some of these open questions with the help of observations in the $g = 3$ Fe I line at 15648 Å of a large, relatively symmetric sunspot. This is one of the first applications of this spectral line to sunspots (cf. Livingston 1991; Kopp et al. 1992; McPherson et al. 1992) and is in many respects exploratory.

2. Observations

A large (51″ × 64″), relatively symmetric sunspot was observed with the McMath telescope, the main spectrograph used in double pass mode and the "Baboquivari" infrared detector on the morning of 10th November, 1990. See Livingston (1991) and Solanki et al. (1992a, hereafter called Paper II) for more details of the setup. In contrast to the data sets analysed by Rüedi et al. (1992a, b, called Papers III & IV, respectively) only the $g = 3$, λ 15648 Å line was recorded. By limiting the observed wavelength range it was possible to obtain more spectra of the sunspot during the period of good seeing. The spectral resolving power of the oversampled data was 150 000 (see Paper II) and the signal-to-noise ratio in the Stokes I continuum was $1 - 3 \times 10^{-3}$. Prior to the analysis the S/N ratio was improved by a factor of approximately 2 through Fourier filtering.

The sunspot belonged to NOAA group No. 6358. It was the following spot of a normal bipolar region and had positive polarity. It was a mature sunspot; the active region was first seen at the east limb on 7th October 1990, with all spots having been born on the far side of the sun, and was last seen, at the west limb, on 12th December 1990. A magnetogram of the active region, obtained on 10th November, is depicted in Fig. 1. The observed sunspot is indicated by the bars. At the time of observation it was near the central meridian: the angle θ between the line-of-sight and the surface normal was 10° ($\mu = \cos \theta = 0.985$).

Three slices (or scans) were made through the spot, two in the solar N–S direction and one in solar E–W direction. Figure 2 shows the umbral and penumbral boundaries of the spot with the approximate positions of the entrance apertures to the spectrograph. 71 spectra in Stokes I and V were obtained. The entrance aperture consisted of a Bowen-type image slicer (each element was 1 × 0.14 mm). The seeing was good and stable. Consequently the effective spatial resolution is estimated to be $2'' - 3''$. The Stokes I and V spectra, after Fourier smoothing, are shown for the three slices across the spot in Figs. 4a,b, 5a,b, and 6a,b. Due to an artifact, the 5th last spectrum of slice 3 was not
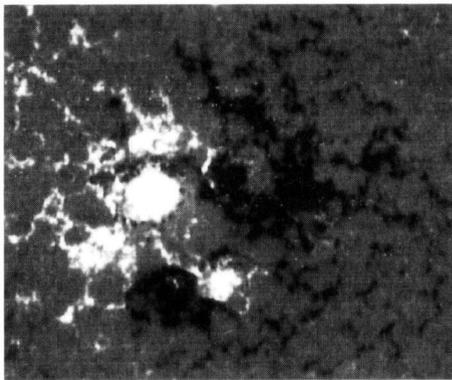
Fig. 1. Detail from a Kitt Peak full-disk magnetogram showing the active region of which the analysed sunspot (marked by the bars) was a member
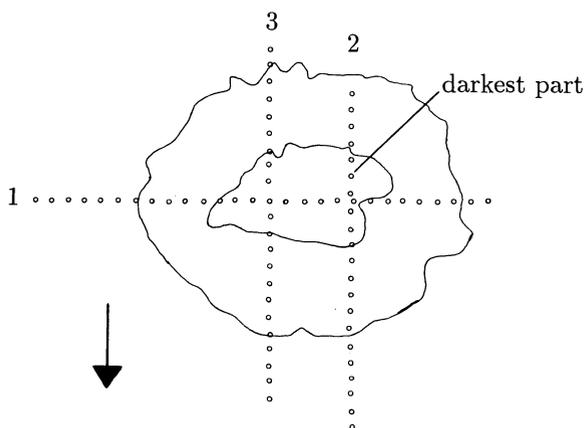

Fig. 2. Contours of the umbral and penumbral boundary of the sunspot. The small circles represent the positions at which spectra were obtained. The three slices through the sunspot are numbered near their starting positions. The arrow points towards disk centre

used for most of the analysis. The continuum intensity normalized to the local photospheric value (defined by the highest I_c value in a particular slice) is plotted in Figs. 4c, 5c and 6c (solid curves). The other curves in Figs. 4c, 5c and 5c represent $1 - 5d$, where d is the normalized depth of either λ 15646.2 Å (0–1 band of CN, Livingston & Wallace 1991, short dashes), or 15650.7 Å (a blend of two lines belonging to the 4–2 band of OH, Wallace and Livingston 1992, long dashes). The former line is seen everywhere on the sun, while the latter is a purely umbral line.

3. Models and method of analysis

In the sunspot the field strength B and the inclination angle γ relative to the line-of-sight are determined by fitting the observed Stokes I and V profiles with synthetic profiles (see Paper II). The fitting has been done either with an inversion code or manually. The manual fitting was required to reproduce, e.g., the complex Stokes V profiles observed outside the sunspot (when multiple

magnetic components are present in the spatial resolution element, cf. Sect. 4.3).

The inversion code used is, like the one described by Keller et al. (1990), based on the non-linear least-squares fitting of Stokes spectra with numerically calculated profiles using the Levenberg-Marquardt algorithm (e.g. Press et al. 1990). However, there are a number of differences. E.g., whereas the Keller et al. (1990) code uses a Runge-Kutta solution (Beckers 1969), the present inversion code uses the Diagonal-Element Lambda Operator, or DELO technique (Rees et al. 1989) and incorporates elements of the code described by Murphy (1990) and Murphy & Rees (1990). In addition, the present code fits the spectral profiles, while the Keller et al. code fits selected line parameters. For the measurement of magnetic parameters using the λ 15648 Å line full profile fitting has undoubted advantages.

The list of all free parameters for the Stokes I and V profiles of a single spectral line reads: The height-independent field strength B, the height-independent angle of inclination γ, the amount of stray light (which is formally treated by introducing a magnetic filling factor α), Doppler shift $\Delta\lambda$, Doppler width of the microturbulent ξ_{mic} and macroturbulent ξ_{mac} velocity distributions, Van-der-Waals fudge factor δ_Γ, combined oscillator strength and abundance $\log gf\epsilon$, and finally the temperature T, which is a function of height. Due to the small temperature sensitivity of λ 15648 Å (see Paper II), we simply use a discrete set of empirical temperature models. More details on these are given later in this section. Note that since only a single spectral line was observed we cannot distinguish between macroturbulent broadening of the σ components and their broadening due to a distribution of field strengths within the spatial resolution element. In the present investigation we have always assumed the field strength to be single valued.

We have never kept all these parameters free simultaneously. For example, it is not possible using a single spectral line to clearly distinguish between the effects of ξ_{mic}, ξ_{mac} and δ_Γ (cf. Holweger et al. 1978). Following Paper II we have chosen $\log gf = -0.7$, $\delta_\Gamma = 2.5$ and $\xi_{mic} = 0.6$ km s^{-1} for the final fits to all the observed spectra.

The temperature stratifications of the models used to fit the data are plotted in Fig. 3. The model names are abbreviations: HSRASP is a quiet-sun model (Gingerich et al. 1971, but see Paper II for more details) used to describe the atmosphere beyond the visible penumbral boundary, as well as the non-magnetic stray-light component of spectra measured within the spot. OS2: The hot component of a 2-component umbral model by Obridko & Staude (1986). A model of approximately this temperature is needed to fit a few profiles just inside the outer penumbral boundary. DF: Penumbral model of Ding & Fang (1989), used to model most penumbral profiles and also some of the profiles just inside the umbral boundary. MSPOTL2: An interpolation between DF and the warmest of the three Maltby et al. (1986) umbral models (model L). The rest of the atmospheric parameters of MSPOTL2 are calculated self-consistently from its $T(\tau)$. The opacity was determined using the ABSKO routine of Gustafsson (1973). MSPOTL2 was needed to model profiles in some of the brighter parts of the umbra (Model L of Maltby et al. was also tried, but was finally not required to reproduce any of the observed profiles). Finally, MSPOTM and MSPOTE, the middle (M) and coolest (E) umbral models of Maltby et al. (1986) were used to fit profiles in the cooler parts of the umbra.

The iterative fitting procedure is assumed to have converged if the reduced χ^2 falls below unity, where χ^2 has its usual meaning,

i.e. the sum of the squared discrepancies from the observations, divided by the degrees of freedom and the uncertainty in the measurements. Whenever possible we determine both γ and α, namely when the line is sufficiently strongly split, $\gamma \gtrsim 30\text{-}40°$ and both Stokes I and V are fit. Then the ratio of the σ-component amplitudes of V to those of I and the ratio of the Stokes I σ-components to its π-component can together be used to diagnose γ and α. For an optically thin line the former ratio equals $2\cos\gamma/(1 + \cos^2\gamma)$, which varies rapidly for $\gamma \gtrsim 30\text{-}40°$, but unfortunately lies close to unity for smaller γ. With our data set we can therefore constrain γ in most of the *umbra* only by first assuming that the stray light there is negligible. In view of the very low stray light values obtained in the outer umbra and inner penumbra this assumption appears quite reasonable. In the *penumbra*, on the other hand, we can accurately determine both the stray light and γ simultaneously.
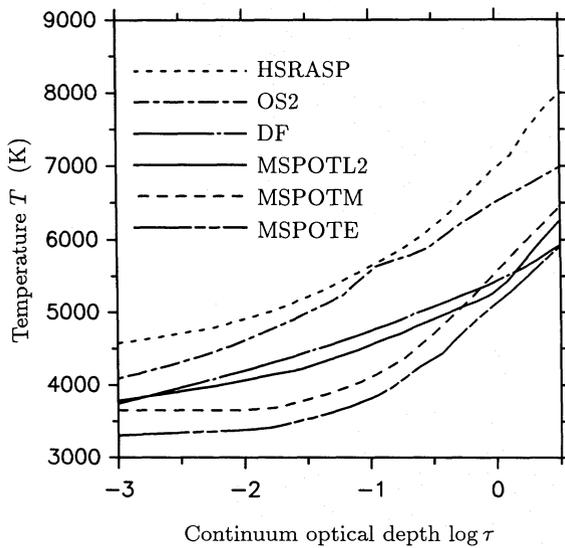

Fig. 3. Temperature T vs. $\log\tau$, logarithmic continuum optical depth at 16 000 Å, of the models used in the present investigation

Whenever possible both the Stokes I and V profiles were fit. However, observed Stokes I profiles whose σ-components could not be clearly distinguished from their π-components were not fit (mainly Stokes I profiles outside the sunspot). Stokes V was not fit when it became highly asymmetric due to instrumental crosstalk from Stokes Q or U. Since the observations were carried out with the McMath main telescope the cross-talk is much smaller than that seen and discussed in Paper IV (where observations obtained with the east auxiliary telescope are analysed) and only becomes significant for $\gamma \gtrsim 85°$. Such a large inclination angle is only reached near the outer edge of the penumbra at the beginning of slices 1,2 and 3. If either Stokes I or Stokes V is analysed alone then it is not possible to distinguish between γ and α. If such profiles lie within the visible outline of the sunspot we have simply assumed γ to be equal to that determined from the nearest profile for which both Stokes I and V could be fit. This assumption was tested and found to be reasonable by comparing with the results obtained near those parts of the penumbral boundary where both I and V were fit (cf. Fig. 8b). Furthermore, the field strength is determined directly from the splitting and is practically independent of the assumed γ. Outside the outer

penumbral boundary more care has had to be taken and different models have been tried (see Sect. 4.5).

Table 1. Sunspot magnetic parameters for $r/r_p \leq 1$

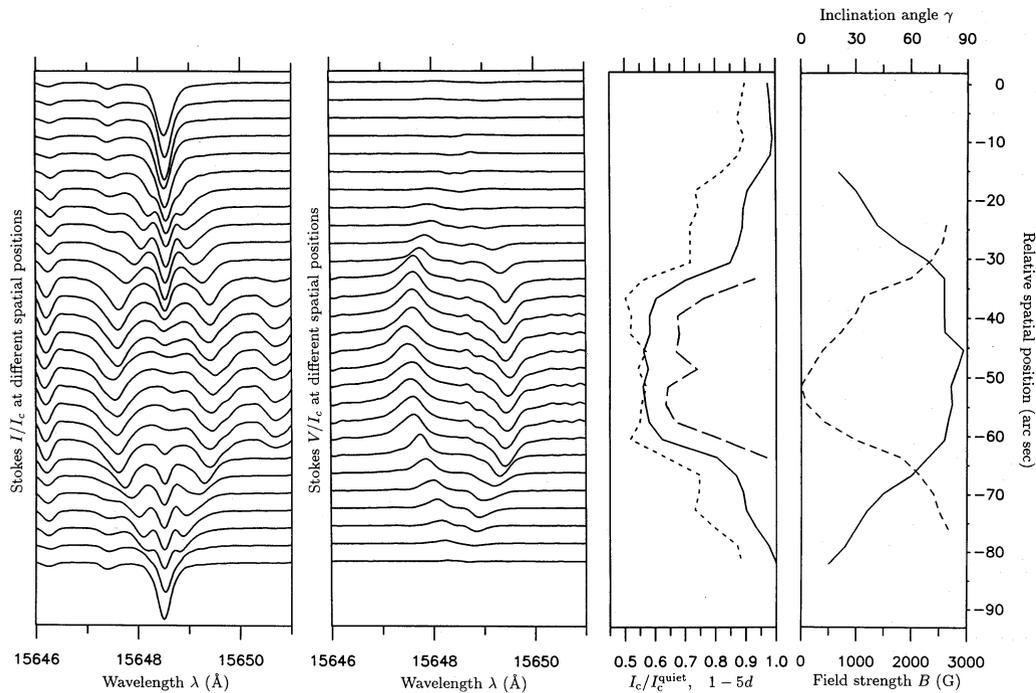| Slice No.	Profile No.	r/r_p	Model	B (G)	γ' (°)
1	7	1.00	OS2	980	—
1	8	0.90	DF	1210	—
1	9	0.80	DF	1430	79
1	10	0.71	DF	1770	77
1	11	0.61	DF	2340	71
1	12	0.51	MSPOTL	2610	61
1	13	0.41	MSPOTL2	2600	37
1	14	0.32	MSPOTL2	2600	32
1	15	0.22	MSPOTL2	2610	25
1	16	0.12	MSPOTL	2940	17
1	17	0.02	MSPOTL	2840	13
1	18	0.08	MSPOTL2	2720	12
1	19	0.19	MSPOTL2	2740	12
1	20	0.30	MSPOTL2	2660	17
1	21	0.40	DF	2600	32
1	22	0.51	DF	2330	56
1	23	0.62	DF	2020	66
1	24	0.73	DF	1510	72
1	25	0.84	DF	1180	75
1	26	0.95	DF	990	80
2	1	0.84	DF	1140	—
2	2	0.73	DF	1400	—
2	3	0.59	DF	1820	66
2	4	0.46	DF	2390	62
2	5	0.43	MSPOTL2	2630	29
2	6	0.31	MSPOTE	3100	10
2	7	0.27	MSPOTL	2790	10
2	8	0.26	MSPOTL2	2520	15
2	9	0.34	MSPOTL2	2470	16
2	10	0.43	MSPOTL2	2380	20
2	11	0.54	DF	2230	29
2	12	0.67	DF	2200	64
2	13	0.73	DF	1620	69
2	14	0.87	DF	1270	74
2	15	0.97	DF	1110	82
3	3	0.92	DF	900	—
3	4	0.83	DF	1170	—
3	5	0.71	DF	1510	66
3	6	0.53	DF	2240	64
3	7	0.45	MSPOTL2	2420	52
3	8	0.34	MSPOTL2	2510	30
3	9	0.29	MSPOTL2	2600	24
3	10	0.23	MSPOTL2	2680	18
3	11	0.27	MSPOTL2	2640	18
3	12	0.38	DF/MSPOTL2	2360	37
3	13	0.45	DF	2010	48
3	14	0.57	DF	1480	69
3	15	0.65	DF	1320	79
3	16	0.78	DF	890	79
3	17	0.90	DF	800	81

Fig. 4. a. Stokes I/I_c along slice No. 1. Each profile has been shifted vertically by a constant amount relative to its neighbour. The topmost profile was recorded at the first point of the slice. **b.** Stokes V/I_c profiles along slice No. 1, ordered and shifted as in Fig. 4a. The zero-level of the V/Ic profiles is placed at the same level as the continuum of the I/Ic profiles (in Fig. 4a) obtained at the same spatial position. **c.** Variation of brightness and temperature indicators along slice No. 1. Solid curve: Continuum intensity I_c, normalized to the average 'quiet sun' value, long dashes: $1 - 5d$, where d is the normalized depth of the 15650.7 Å line, short dashes: $1 - 5d$ of CN 15646.2 Å. The values plotted at a vertical position corresponding to the continuum level of one of the Stokes I spectra in Fig. 4a were derived from that spectrum. **d.** Magnetic field strength B (solid) and inclination angle of the magnetic field to the line of sight γ (dashed) along slice No. 1. Only the γ values determined from a combination of Stokes I and V are plotted
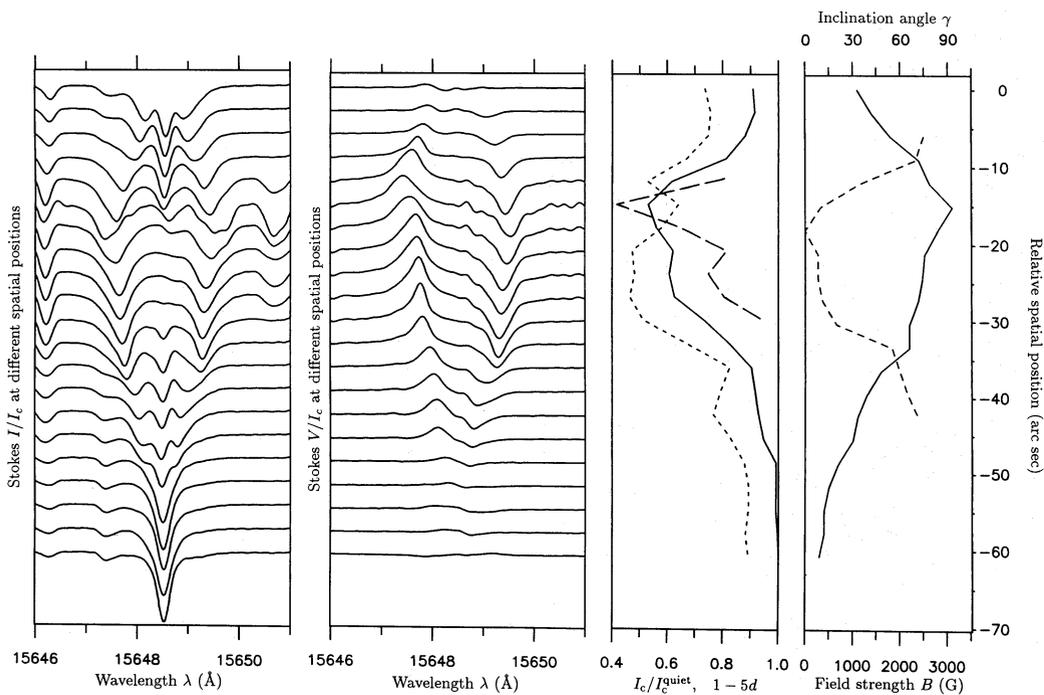
Fig. 5a-d. Same as Fig. 4, but for slice No. 2 which passes through the darkest part of the sunspot; sixth Stokes I and V profiles from the top. Note their jagged shapes due to molecular blending
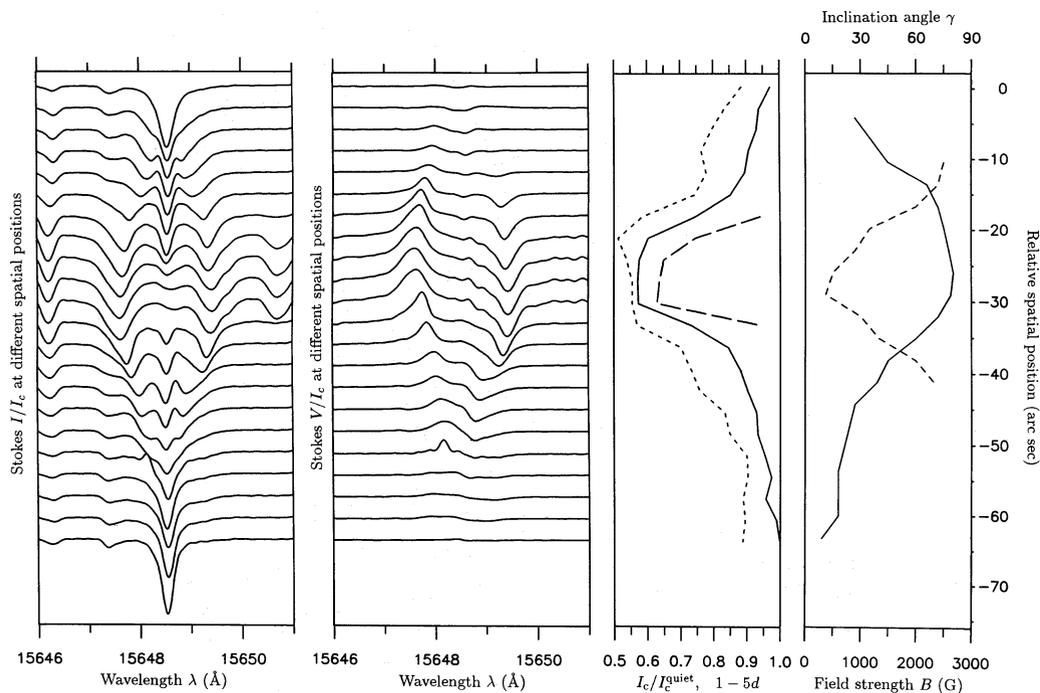
Fig. 6a-d. Same as Fig. 4, but for slice No. 3

4. Results

4.1. Sunspot slices

The field strength B (solid) and the inclination angle γ (dashed) along each of the three slices through the sunspot, as derived from fits to the observed profiles, are plotted in Figs. 4d, 5d and 6d, respectively. The field strength can be measured directly from the splitting, so that it is reliably determined for many more profiles than the inclination angle (Sect. 3). The estimated uncertainty in the measured field strength is approximately 50 G in most of the sunspot, but reaches 100 G in the darkest part of the umbra, as well as outside the outer penumbral boundary. The relative inaccuracy of the measured B values outside the penumbra is mainly due to the low B, coupled to the low magnetic signal there (see Sect. 4.5). In the dark part of the umbra the main cause of the uncertainty is the appearance of molecular lines which blend into and distort the profile of λ 15648 Å. Thus the distortions in the most strongly split profile of our sample (6th from the top in Fig. 5) are mainly due to blends and not to noise. One of these blends lies close to the position of the π-component. Thus the Stokes I profiles in the cooler parts of the umbra give the appearance of having a π-component that is shifted relative to the σ-components. If the presence of the blend were not known then such an observation would be interpreted as the presence of non-magnetic material in the umbra flowing away from the observer at a velocity of several km s^{-1}.

However, fortunately the blending line is Zeeman sensitive and the Stokes V profiles measured in the umbra show the tell-tale signs of a weakly Zeeman split line at the position of the 'shifted π-component'. One measured umbral profile exhibiting this blend is shown in Fig. 7a (solid curves), together with the best fits (dashed). The quality of the fit is typical of most umbral profiles. Note also the asymmetry between the two σ-components, which is mainly due to a blend in the blue σ-component. The blending line is visible in Fig. 7b as the separate peak bluewards

of Fe I 15648 Å . It is present in all spectra, but blends with the blue σ-component of the $g = 3$ line only for large field strengths.

The results obtained within the visible boundary of the sunspot are given in Table 1, which lists the slice number, the spectrum number within each slice, r/r_p, the model atmosphere used to fit the profiles, B and γ' (the inclination of the magnetic field to the vertical).

4.2. Radial dependence of B

We can combine the measurements of the three slices by plotting field strength and inclination angle vs. radial distance r from the geometrical centre of the whole sunspot (its 'centre-of-gravity'). Since the sunspot is not completely symmetric we scale all r values by the radius r_p of the local outer penumbral boundary (i.e. the penumbral boundary in the same direction as the observed region seen from the geometric centre of the spot). The field strength B is plotted in Fig. 8a as a function of r/r_p. We wish to stress two points in Fig. 8a.

a) Most of the scatter around the mean curve is intrinsic to the sunspot. To illustrate this we have represented the data points along each half of each slice by a different symbol. In some directions (e.g. dots) the field drops off more slowly with r/r_p than in others (e.g. open circles). There are also some anomalous points, which probably are again due to intrinsic properties of the spot, e.g. the point marked 'Z' near $r/r_p = 0.3$ with $B > 3000$ G corresponds to the darkest part of the umbra.

b) The field strength at the outer penumbral boundary is accurate to approximately 50 G, so that the scatter there is again mainly solar in origin. Note also that the field strength values at $r/r_p > 1$ have been determined from the splitting of the V profiles and therefore represent the true field strengths (see Sect. 4.5).
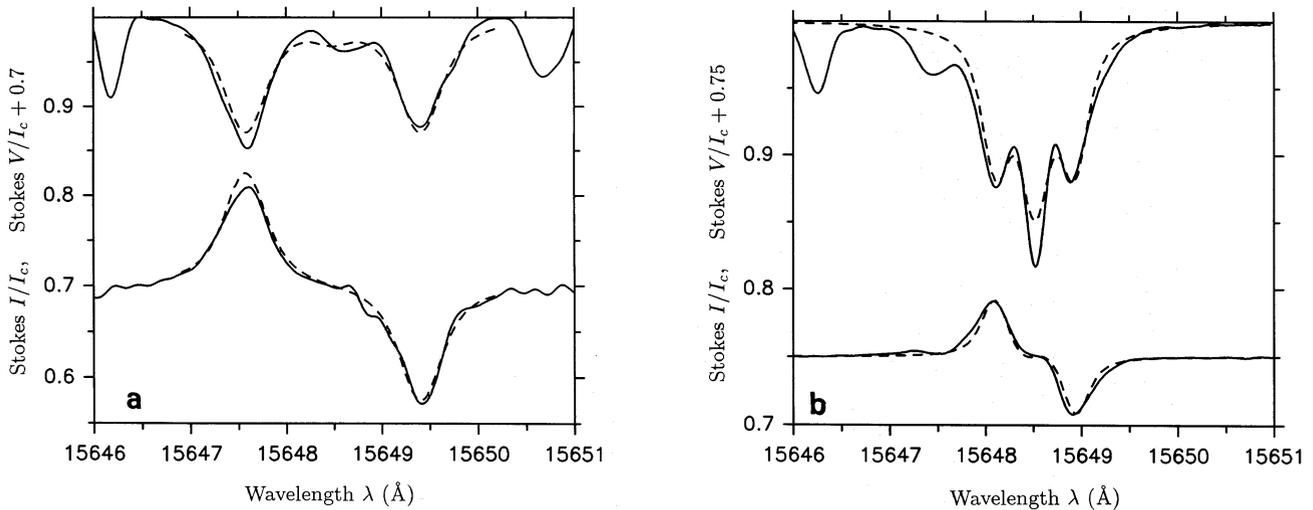
Fig. 7. Measured (solid) and synthetic (dashed) profiles of Stokes I (top) and Stokes V (bottom) of Fe I 15648 Å. **a.** An umbral profile. The quality of the fit is typical. The difference between observed and synthetic profiles in the blue wing is due to the presence of a blend. **b.** A penumbral profile which allowed only a fit of below average quality. Note in particular the excess width of the measured σ-components

4.3. Radial dependence of γ'

In Fig. 8b we plot the inclination γ' of the field lines to the vertical. The transformation of γ into γ' entails a rotation of the coordinate system by the heliocentric angle of the observations $\theta = 10°$. Since an unknown azimuth φ of the field is required to carry out this transformation we assume the horizontal component of the field to be radial. For a relatively symmetric sunspot observed departures from a radial field are smaller than $10 - 20°$ (Landi Degl'Innocenti 1979; Kawakami 1983; Lites & Skumanich 1990). The uncertainty in φ can, in the worst possible case (φ is in error by 180° and $\varphi = 0°$ or 180°), introduce a maximum error of 20° into γ. Large errors in φ are expected mainly in the inner umbra where the field is nearly vertical and a small difference in the direction of the field vector can correspond to a large difference in φ. We suspect that this uncertainty is to a large part responsible for the larger scatter in γ' values in the umbra, as compared to B values. The horizontal dashed line in Fig. 8b separates the reliable γ' values (above the line) from the somewhat less reliable ones (below it).

In the penumbra only extremely large horizontal twists of the field, for which there is no observational evidence, would lead to any significant error in γ'. We have tested the effect of a simple twist by assuming that all φ values are wrong by the same amount and then redetermining γ' from γ. The presence of a twist leads to a greater scatter between the data points in the various 'half-slices' for γ' than for B. The scatter is smallest for a minor or absent twist. In addition, γ' at the outer penumbral boundary, for which we obtain $\gamma' (r/r_p = 1) = 82 \pm 4°$, should be little affected by the uncertainty in φ. This inclination is somewhat larger than that found by e.g. Adam (1990) and Lites & Skumanich (1990), but is consistent with γ values derived from the superpenumbral magnetic canopy (see Sect. 4.5). Another sign that the derived γ' values near the outer penumbral boundary are correct is the fact that the V profile disappears almost completely at the beginning of slices 1, 2 and 3; only a minute residual Stokes Q-shaped profile is left due to instrumental cross-talk. From the upper limits on the V amplitudes at these positions (given by the amplitudes of the Q-shaped profiles) we can determine lower limits to γ' at $r/r_p = 1$. We obtain $\gamma' (r/r_p = 1) > 80°, 77°$ and 74° for the three

slices, respectively. $\gamma' (r/r_p > 1)$ has been determined by other means than directly from profile fits and is discussed in Sect. 4.5.

4.4. Stray light

In the penumbra we have treated stray light as an independent parameter. Except near the outer edge of the penumbra we have been able to reproduce observed Stokes I and V profiles without the need of any stray light, i.e. with 100% magnetic filling factor in the resolution element. The filling factor should be accurate to within 5%. At $r/r_p \gtrsim 0.8$ the effects of stray light begin to be felt. However, except for a single point the filling factor is always well above 80% within the sunspot; one profile at $r/r_p \approx 0.9$ requires 25% stray light to be reproduced. This confirms that the seeing was good during the observations. More importantly, this observation implies that in the lower photosphere very little if any non-magnetic gas is present in the inner and central penumbra ($\lesssim 5\%$ of the volume) and $< 10 - 20\%$ in the outer penumbra (cf. Deming et al. 1991). Due to the relative temperature insensitivity of the $g = 3$ line and the weak dependence of the Planck function on temperature at $1.5\,\mu m$ these limits on the filling factors should be relatively reliable even if the temperature is not the same in the hypothetical non-magnetic component as in the magnetic component.

4.5. The superpenumbral canopy

All the B values in Fig. 8a at $r/r_p > 1$ have been derived from Stokes V alone because Stokes V is completely split for much lower field strengths than Stokes I and because Stokes I is dominated by light from the field-free photosphere. Only on the diskward side of the sunspot in slices 2 and 3 are the Stokes V profiles sufficiently free of instrumental cross-talk to be used to determine B for $r/r_p \gtrsim 1.2$.

Initially we fit the V profiles at $r/r_p > 1$ using a homogeneous field with $\gamma = \gamma(r/r_p = 1)$. This is not a critical assumption for the determination of the field strength, since it is relatively independent of γ. The fits from this initial analysis lead to the following results:
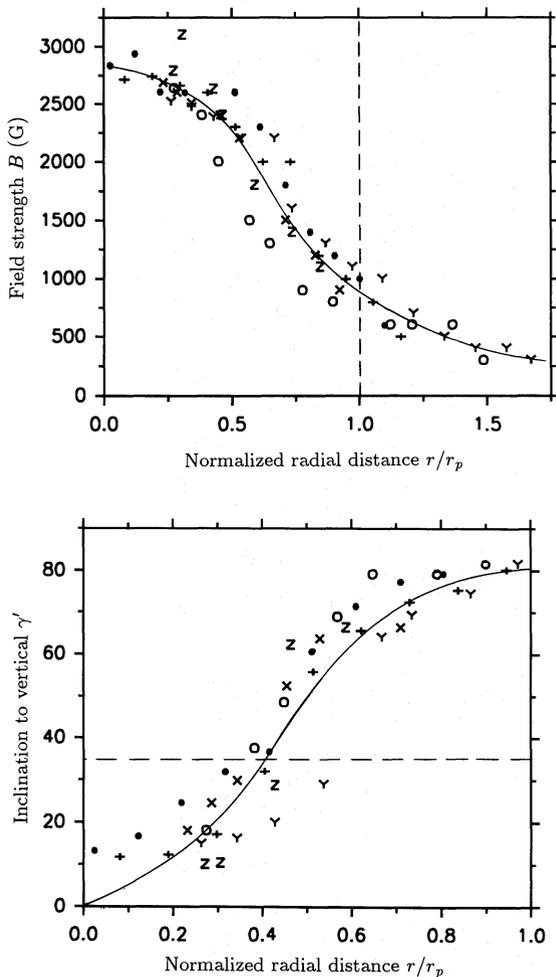
4. The weak-field component has everywhere the same polarity as the sunspot, while the strong-field component can have either polarity and is sometimes completely absent.

Figure 9 shows examples of Stokes V profiles at $r/r_p > 1$. Plotted are the last four profiles (from top to bottom) of slice 2 in Fig. 9a and the last four profiles of slice 3 in Fig. 9b. The solid profiles have been observed, the dashed ones are synthetic. The topmost profile in Fig. 9a and the lowest in Fig. 9b can be reproduced with a single magnetic component, the others all require two magnetic components. Note the opposite polarity of the V profile due to the strong-field component in the lowest spectrum in Fig. 9a, as compared to the other profiles. Also note that the polarity of the weak-field component remains the same.

The above results suggest the following identification. The weak-field component is an extension of the sunspot's magnetic field beyond its outline: it is the magnetic structure of the superpenumbra. The strong-field component is due to small-scale concentrated magnetic features, i.e. magnetic elements. We adopt this interpretation as the basis for the rest of the analysis. Note that in Fig. 8a only the field strength of the weak-field component has been plotted.

In a second step we model the sunspot component at $r/r_p > 1$ by a height-independent field strength, but represent the facular component by flux-tube models similar to the ones described in Papers II and III. This approach leads to improved fits (the fits in Fig. 9 were actually obtained with this model). In Table 2 we list some of the parameters of the fits to profiles at $r/r_p > 1$ using the improved model. Columns 3 and 4 contain the field strength and 'filling factor' of the sunspot component. The field strengths derived for the flux-tubes are listed in column 5. There is little danger of misidentifying the two magnetic components since the difference in field strength is of the order of 1000 G. The results listed in Table 2 were all aquired by assuming that all components are described by the HSRASP. To test this assumption we have also used other atmospheric models to describe the magnetic components. The field strength is not affected by the chosen temperature. Although the filling factors can be affected, its trend with r/r_p is not changed.

Although a height-independent field reproduces the sunspot component, it is difficult to envisage a physically reasonable geometry compatible with such a field. We therefore propose a geometrically different interpretation of the observations: We assume a canopy-type structure, i.e. we assume that above a certain height z_c (the canopy base height) the atmosphere is filled with a field connected to the sunspot, while below this height the atmosphere is mainly field free and only the fields of the magnetic elements are present. This interpretation is consistent with the analysis of Giovanelli (1980) and Giovanelli & Jones (1982), who deduced the presence of a superpenumbral canopy from magnetograms of chromospheric and photospheric lines. Above the canopy base there are two magnetic components, a homogeneous, almost horizontal sunspot field covering most of the surface and an almost vertical field due to the flux tubes. In our simple model the flux-tube field is allowed to flare out until it reaches a strength equal to the sunspot field forming the canopy. Above that height the field is kept vertical and constant. The temperature structure in all the components of this model is assumed to be that of the HSRASP at the corresponding optical depth. The gas pressure in the magnetic components is adjusted so as to preserve equilibrium at the sharp boundaries to the field-free gas.
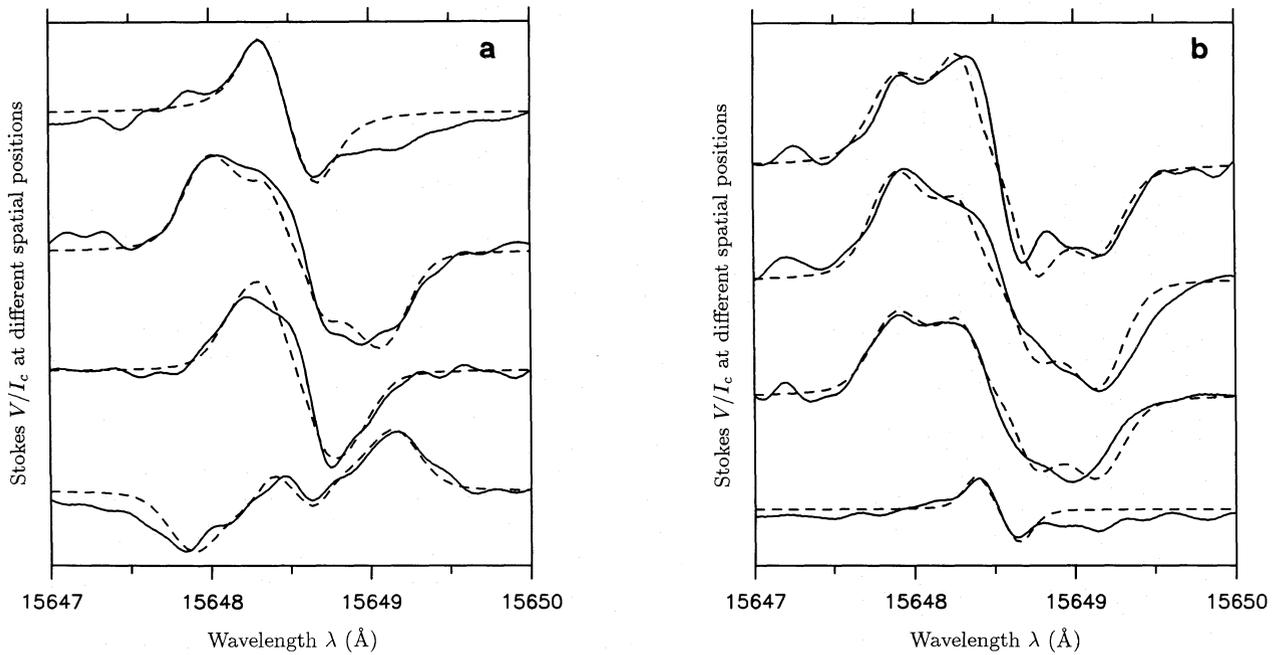

Fig. 8. a. Magnetic field strength B vs. radial distance r from the geometrical centre of the sunspot normalized to the outer penumbral radius r_p in the relevant direction (compare with Fig. 2): r/r_p. The symbols represent different halves of the 3 sunspot slices. Dots = left (first) half of slice 1, plusses = right (second) half of slice 1, 'Z' = limbward half of slice 2, 'Y' = diskward half of slice 2, 'X' = limbward half of slice 3, open circles = diskward half of slice 3. The solid curve is an eyeball fit to the data. **b.** Angle of inclination γ' to the solar surface normal vs. r/r_p. The symbols have the same meanings as in Fig. 8a. The points below the horizontal dashed line are of lower accuracy than the rest. The solid curve is an eyeball fit to the data which is forced to go through the origin

1. Only some of the V profiles can be reproduced with a single magnetic component, the others show distinct signs of two magnetic components, a weak-field and a strong-field component, typical of many of the plage profiles analysed in Paper III.

2. The field strength of the magnetic component with the weaker field decreases steadily with increasing r/r_p in a manner which is entirely consistent with the $B(r/r_p)$ dependence for $r/r_p < 1$, while that of the strong-field component shows no recognizable dependence on r/r_p.

3. The 'non-magnetic stray light' affecting the weak field magnetic component increases steadily with distance from the sunspot, while the 'stray light' affecting the strong-field component shows no particular dependence on r/r_p.

Fig. 9. Observed (solid) and calculated (dashed) Stokes V profiles beyond the outer edge of the penumbra ($r/r_p > 1$). Profiles at the top of a frame are closest to the penumbral boundary, profiles at the bottom are furthest away. **a.** Last 4 profiles of slice No. 2. **b.** Last 4 profiles of slice No. 3

Table 2. Sunspot magnetic parameters for $r/r_p > 1$ derived from Stokes V

Slice No.	Profile No.	B (G) sunspot component	f (%) sunspot component	$B(z=0)$ (G) flux tube component	B (G) canopy	z_c (km)	γ' (°) at canopy base
2	16	1000	65	–	900	100	84
2	17	700	35	–	700	270	86
2	18	500	27	–	600	340	88
2	19	400	25	1500	500	360	89–90
2	20	400	10	1100	500	380	89–90
2	21	399	5	−1600	400	420	89
3	18	?[1]	70[2]	–	?[1]	200[2]	83[2]
3	19	600	33	1600	600	310	87
3	20	600	23	1600	500	340	89–90
3	21	600	21	1600	500	350	89–90
3	22	300	7	–	300	390	89

[1]   Due to an artifact only one of the wings of the V profile can be used. Therefore B cannot be directly determined. However f, respectively z_c and γ'_c do not depend strongly on B and can be determined by using an interpolated value of B.
[2]   Obtained assuming $B = 800$ G.

We find that by varying z_c and B of the canopy we can reproduce the observed Stokes V profiles practically as well as in Fig. 9 without having to introduce additional stray light for the canopy component. In this model z_c determines the amplitude and B(canopy) determines the splitting of the sunspot component of the observed profiles. Similarly, the filling factor α and the field strength $B(z=0)$ of the flux tubes determine the amplitude and splitting, respectively, of the flux-tube component of the profiles. $z=0$ corresponds to the $\tau_{5000} = 1$ level in the quiet sun. The

canopy field strengths and base heights giving the best fits are listed in columns 6 and 7 of Table 2, respectively. The $B(z=0)$ of the flux tubes remain unchanged, and are listed in column 5.

In Fig. 10 z_c is plotted vs. $r - r_p$, the distance from the outer edge of the penumbra. The solid curve is obtained from data in the second slice, the dashed curve from the third slice. The canopy base of this sunspot first increases slowly until it reaches approximately $300 - 400$ km above $z = 0$ after which it remains almost constant. Surprising is the similarity between the
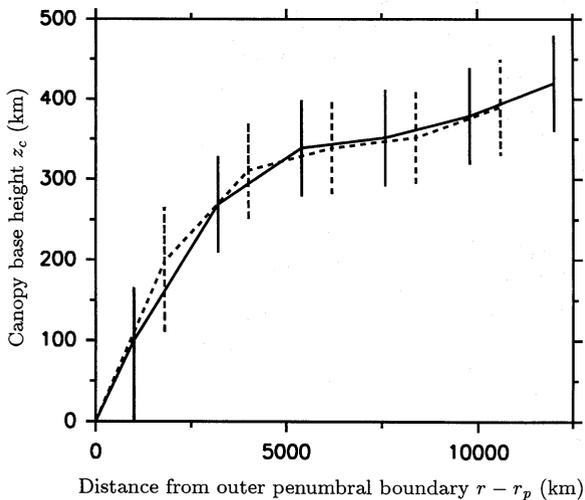
Fig. 10. Base height z_c of the superpenumbral magnetic canopy vs. distance from the outer boundary of the penumbra, $r - r_p$. Solid and dashed curves represent z_c derived from slices 2 and 3, respectively

two curves. It confirms our suspicion that the statistical errors in the determined z_c are rather small, of the order of 20–30 km for most points. This is due to the extreme sensitivity of the V profile amplitude to z_c, which in turn has to do with the approximately exponential decay with z of the contribution function above its peak. Thus, even a small change in z_c can significantly affect the area of the contribution function above z_c, which is directly proportional to the amplitude of Stokes V.

The error bars in Fig. 10, which are considerably larger than the statistical error of 20–30 km, reflect our estimate of possible systematic errors.[1] These systematic effects are mainly due to uncertainties in γ and in the thermodynamic structure of the atmosphere above and below the canopy. We have estimated the uncertainties by varying these parameters within reasonable limits. Note that at the positions at which z_c is low and lies closer to the height of the contribution maximum to Fe I 15648 Å, the error bars are larger, since the Stokes V amplitude then does not depend so sensitively on z_c. Horizontal error bars due to positioning errors, etc. have not been plotted. We estimate such errors to be approximately 1000 km.

Once we have derived z_c vs. $r - r_p$ we can determine γ' of the field at the canopy base by requiring that $z_c(r)$ follows a field line. This γ' in general does not agree perfectly with the γ' originally assumed when deriving z_c and B. Therefore we iterate the whole process, i.e. using the new γ' we redetermine z_c and B in the canopy. From these we can determine a new γ' and so on until convergence. Since the original estimate of γ' was relatively close to the final value our model converged to within the accuracy allowed by the data after a single iteration. The B and z_c values listed in columns 6 and 7 of Table 2 are the converged values. The converged B values do not differ at all and the z_c values differ by less than the error bars from the initially determined ones. The converged γ' are listed in column 8 of Table 2. At $r \approx r_p$ they are compatible with the γ' values determined directly from the I and V profiles.

---

[1] The difference between the two curves is much smaller than the error bars since the systematic errors probably affect both curves in the same manner.

5. Discussion and conclusion

We have presented observations of a relatively symmetric sunspot using the Fe I $g = 3$ line at $\lambda\ 15648$ Å and have derived various parameters of the magnetic field. For much of the analysis we have used an inversion code which derives magnetic parameters by fitting observed profiles with profiles based on the numerical solution of the Unno-Rachkovsky equations in realistic atmospheres. In the following we review the results, briefly compare them with earlier investigations and discuss some of their consequences.

5.1. Field strengths

The $\lambda\ 15648$ Å line is well suited to determine field strengths in sunspots. The accuracy of the derived field strengths varies between 50 and 100 G. This line bridges the gap between lines in the visible (e.g. Fe I 6302.5 Å) and the $12\,\mu m$ emission lines. Visible lines can easily measure umbral fields, but do not have the Zeeman sensitivity to accurately determine the field strength in the outer penumbra, whereas the $12\,\mu m$ lines measure the field strength with great accuracy in the penumbra, but are not seen in emission in all but the brightest parts of the umbra (Deming et al. 1988). The $\lambda\ 15648$ Å line is complementary to the others in two ways: Firstly it is formed deeper than the other Zeeman sensitive lines. The height of formation of the $12\,\mu m$ lines now appears to be just below the temperature minimum (Chang et al. 1991; Carlsson et al. 1992), while the $1.5\,\mu m$ line is formed close to the $\tau_{5000} = 0.1$ level (Grossmann-Doerth et al. 1989). Secondly, it covers the whole range of temperatures and field strengths found in sunspots. Only in the very coolest part of the umbra does its accuracy begin to deteriorate due to the appearance of weak, probably molecular blends. In the present spot these blending lines do not affect the measured field strengths significantly, but in very cool umbral cores they make the determination of the field strength without detailed profile fitting very uncertain (cf. Fig. 5 of Paper II). We warn particularly about one such blending line, which lies close to, but not exactly at the rest position of the π-component of $\lambda\ 15648$ Å. It can easily be misinterpreted as a shifted π-component if only Stokes I is measured.

The average radial dependence of the field strength is similar to previously published results based on visible (e.g. Beckers & Schröter 1969; Wittmann 1974; Kawakami 1983; Adam 1990; Lites & Skumanich 1990), 1.5 μm (McPherson et al. 1992), or $12\,\mu m$ spectra (Deming et al. 1988). Small differences in shape to, e.g., the findings of Lites & Skumanich — the shape of their mean curve is smoother — may have to do with intrinsic differences between the observed spots, but are also to be expected due to the lower spatial resolution of the Stokesmeter II data analysed by Lites & Skumanich (1990). The highest field strength measured in the investigated sunspot is approximately 3200 G, and coincides with its darkest part. There is no unique radial dependence of B, with $B(r/r_p)$ behaving slightly differently in different directions.

The field strength at the outer penumbral boundary lies between 800 and 1000 G, depending on the location along the boundary. This is compatible with results obtained with the $12\,\mu m$ lines (Deming et al. 1988), but is larger than values obtained in the visible, except the $B(r/r_p = 1) = 1000 - 1200$ G found by Beckers & Schröter (1969). The good agreement between the $12\,\mu m$ and $1.5\,\mu m$ lines, which sample different heights, suggests that dB/dz is very small at $r \approx r_p$.

5.2. Inclination angle

The general radial dependence of the inclination angle is also similar to results obtained in the visible. The angle of inclination γ' to the surface normal at the outer penumbral boundary is found to be $\gamma' = 82 \pm 4°$ from σ-to-π and V-to-I ratios. This value is in good agreement with the $\gamma'(r/r_p = 1)$ derived from the gradient of the base of the superpenumbral magnetic canopy ($\gamma' \approx 83$–$84°$). γ' values at the outer penumbral boundary derived by other investigators lie between 90° for older investigations (e.g. Beckers & Schröter 1969; Wittmann 1974) and $70 - 80°$ for newer ones (Kawakami 1983; Adam 1990, Lites & Skumanich 1990).

The $\gamma' \approx 90°$ values of older observations are probably an overestimate due to an insufficient correction for stray light, which is particularly acute near $r/r_p = 1$ (cf. Stenflo 1985).

According to magnetohydrostatic models of axially symmetric sunspots (e.g. Pizzo 1986; Jahn 1989), $\gamma'(r/r_p = 1)$ is a function of height: lines formed higher in the atmosphere, such as the visible lines, should give a smaller γ' value than λ 15648 Å. A rough estimate of the expected difference in γ', assuming a monopole model for the sunspot magnetic field (see Sect. 5.3), gives $\Delta\gamma' \approx 1 - 2°$. This is too small to reconcile the differences. Therefore, either the sunspot we have observed is intrinsically different from some of the others, or there are systematic errors of the order of 5° in either the visible or the infrared γ' determinations, or our simple monopole model is incorrect. Although we are hampered by the absence of Stokes Q and U observations, we find $\gamma' \gtrsim 80°$ using 2 independent techniques. Note in particular that if $\gamma'(r/r_p = 1) = 75°$ then the canopy base 3″ beyond r_p (i.e. where the next spectrum is obtained) would lie above 500 km, which is so high that we would not be able to detect the superpenumbral canopy at all using λ 15648 Å.

5.3. Superpenumbral canopy

We can follow the magnetic field of the sunspot well beyond its outer penumbral boundary. $B(r/r_p > 1)$ is well represented by a magnetic monopole lying at the solar surface, i.e. $B(r) \sim 1/r^2$, which suggests that no additional magnetic flux appears or disappears through the solar surface at $r > r_p$. See Solanki & Schmidt (1992) for a more detailed and exact analysis. The measured field becomes almost horizontal and is geometrically best represented by a canopy with a lower boundary lying mainly in the upper photosphere. In the following we discuss the consequences of our analysis at $r > r_p$.

1. Nowhere in the infrared data do we see any signs of a reversal of the magnetic polarity of the superpenumbral field within 1.7 sunspot radii. Thus we do not see any direct signs of a return flux along the two analysed slices. In addition, the $1/r^2$ dependence of B also conflicts with a substantial return flux at $r/r_p > 1$. The presence of such return flux has been proposed by Osherovich (1982), Flå et al. (1982) and Osherovich & Garcia (1989) on the basis of magnetohydrostatic modelling of sunspots.

The evidence against return flux is further strengthend by comparing our observations with those of Giovanelli & Jones (1982). They find that, while lines sampling the upper photosphere and chromosphere (Fe I 8688 Å and Ca II 8542 Å, respectively) show extended diffuse fields around the sunspot, magnetograms in lines formed in the low photosphere (e.g. C I 9111 Å) only show fields that are spatially localized to the sunspot and to a

distinct facular network, contrary to the expectations of return-flux theory.

By combining our observations with those of Giovanelli & Jones (1982) and by assuming that the qualitative properties of the field at $r/r_p > 1$ are relatively universal for sunspots, we can rule out the presence of any significant (local) return flux in sunspots. The model of Osherovich (1982) and of Flå et al. (1982) can therefore be ruled out (cf. Solanki & Schmidt 1992).

2. The paradox that we detect a magnetic structure present only in the upper photosphere using a line that obtains its main contribution much lower is resolved by considering the high Zeeman sensitivity (or 'Zeeman resolution', cf. Deming et al. 1988) of λ 15648 Å. Although the canopy — with $B \lesssim 700 - 800$ G — may only contribute a minor amount to the observed Stokes V profile, this contribution can be spectrally easily distinguished from the contribution of kG flux tubes and the possible contribution of light from the penumbra and umbra smeared to the observed position by seeing (800 G $\lesssim B \lesssim$ 3000 G). Lines in the visible lack the necessary Zeeman sensitivity, so that they cannot readily distinguish between the various sources (but see below). Therefore near disk centre the weak Stokes V signal of a line in the visible due to the canopy is easily swamped by the signal from the other two sources, particularly since, due to its small field strength, the canopy produces a smaller Stokes V signal in the visible than in the infrared.

Nevertheless, we do expect that a visible line formed in the middle photosphere is affected differently by the presence of an almost horizontal canopy than, e.g., by small vertical flux tubes. For example, the $\sqrt{Q^2 + U^2}/V$ ratio due to the two magnetic structures is quite different. In a region in which a superpenumbral canopy and small flux tubes coexist the expected inclination angle derived from measurements of $\sqrt{Q^2 + U^2}/V$ is expected to lie between that of the two components. This effect may be partly responsible for the results of Solanki et al. (1987). They found that the fields of small flux tubes in solar active regions are more strongly inclined to the vertical than predicted by theory (Schüssler 1986, 1990). Since the observations analysed by Solanki et al. (1987) were obtained not too far from sunspots they may well be seeing the combination of nearly vertical flux tubes and a superpenumbral canopy.

The same effect, but now working in the opposite direction, may well lead to the measurement of a too vertical field at the outer penumbral edge if visible lines are observed with not very high spatial resolution (which is the case for the investigations by Kawakami 1983 and Lites & Skumanich 1990). The scattering of light from vertical flux tubes into the penumbra can conceivably lead to an error of a few degrees in γ' of the penumbral field near $r/r_p = 1$. This may explain any remaining difference between γ' ($r = r_p$) derived by us and the investigators mentioned above (cf. Sects. 4.2 and 5.2).

The disadvantage of studying the superpenumbral canopy with a line formed at a low altitude is that the canopy cannot be followed for a similar distance from the spot as with an upper photospheric or lower chromospheric line observed at a similar S/N ratio. In this respect the 12 μm lines would appear to be ideal. Indeed, the data of Deming et al. (1988, 1991) show continuously declining Zeeman splitting and fractional polarization well beyond $r/r_p = 1$, which is consistent with the presence of a magnetic canopy slowly rising higher in the atmosphere with increasing r/r_p.

3. Our observations were made almost at solar disk centre, while previous observations of magnetic canopies have all been

made near the solar limb (see e.g. the review by Jones 1985). Therefore with λ 15648 Å it is now possible to measure superpenumbral canopies over the whole solar disk.

4. Using λ 15648 Å the field strength in the canopy can be determined out to the r/r_p value at which it drops to $300 - 400$ G. With an accurate 1.5 μm line ratio it may in future be possible to measure even lower field strengths, as outlined in Paper II.

5. The large Zeeman sensitivity of λ 15648 Å and the large contrast between B in magnetic elements (near $z = 0$) and in the magnetic canopy allows us to detect the presence of magnetic elements within the same spatial resolution element as the superpenumbral magnetic canopy and to determine their field strengths. Previously the canopy could only be detected at positions where no fields were present in the lower photosphere. The magnetic element $B(z = 0)$ values are concentrated around $1500 - 1600$ G with one value of 1100 G. These values are similar to the ones measured in Paper III, suggesting that the strong fields cospatial with the canopy are due to normal flux tubes. The geometry of the canopy implies that the flux tubes exist as separate entities only below the magnetic canopy and merge with it at its base height. The structure of the field in the vicinity of such a merger is not clear from our observations, nor is it easy to predict without detailed modelling since the field strengths of the two components are not expected to be too different at the height at which they meet.

6. Finally, if no spatial slices are made then it is very difficult to distinguish between the signature of a superpenumbral canopy and of a spatially localized patch of weak field in the lower photosphere from Stokes I and V profiles of λ 15648Å alone. Consequently we cannot rule out that at least some of the weak fields detected in Paper III are parts of superpenumbral canopies.

5.4. Magnetic filling factor

Our observations set a lower limit of approximately 95% on the magnetic filling factor in the central part of the penumbra and approximately 80% in the outer penumbra. This lower limit rules out that substantial parts of the penumbra are field-free, or that the lower penumbral boundary is raised by more than approximately 200 km above the $\tau_{5000} = 1$ level (τ_{5000} is the continuum intensity at 5000 Å). The latter conclusion places constraints on a proposed penumbral canopy (Moore 1981; Cram et al. 1981; Giovanelli 1982).[2] Note that z_c as derived from our data reaches 150-200 km, the value quoted by Giovanelli at $r = r_p$, within 3″ of the outer penumbral boundary. Since he can detect a canopy only outside the sunspot and the effective spatial resolution of his data is lower than this, our analysis (which assumes no penumbral canopy) is compatible with his data.

5.5. Conclusion

The present paper demonstrates the potential of Fe I 15648Å as a diagnostic of sunspot magnetic fields, based upon observations of a simple sunspot. Another diagnostic, namely the relationship between field strength and temperature within a sunspot is investigated in Paper VI of the present series (Solanki et al. 1992b) and by Kopp et al. (1992).

---

[2]   The penumbral canopy (at $r/r_p < 1$) should not be confused with the superpenumbral canopy (present at $r/r_p > 1$) discussed in Sects. 4.5 and 5.3.

References

Adam M.G., 1990, Sol. Phys. 125, 37

Auer L.H., Heasley J.N., House L.L., 1977, Sol. Phys. 55, 47

Balasubramaniam K.S., West E.A., 1991, ApJ 382, 699

Beckers J.M., 1969, Sol. Phys. 9, 372

Beckers J.M., Schröter E.H., 1969, Sol. Phys. 10, 384

Carlsson M., Rutten R.J., Shchukina N.G., 1992, A&A 253, 567

Chang E.S., Avrett E.H., Mauas P.J., Noyes R.W., Loeser R., 1991, ApJ 379, L79

Cram L.E., Nye A.H., Thomas J.H., 1981, in The Physics of Sunspots, L.E. Cram, J.H. Thomas (Eds.), National Solar Obs., Sunspot, NM, p. 384

Cram L.E., Thomas J.H., 1981, *The Physics of Sunspots*, National Solar Obs., Sunspot, NM

Deming D., Boyle R.J., Jennings D.E., Wiedemann G., 1988, ApJ 333, 978

Deming D., Hewagama T., Jennings D.E., Wiedemann G., 1991, in Solar Polarimetry, L.J. November (Ed.), National Solar Obs., Sunspot, p. 341

Ding M.D., Fang C., 1989, A&A 225, 204

Flå T., Osherovich V.A., Skumanich A., 1982, ApJ 261, 700

Gingerich O., Noyes R.W., Kalkofen W., Cuny Y., 1971, Sol. Phys. 18, 347

Giovanelli R.G., 1980, Sol. Phys. 68, 49

Giovanelli R.G., 1982, Sol. Phys. 80, 21

Giovanelli R.G., Jones H.P., 1982, Sol. Phys. 79, 267

Grossmann-Doerth U., Knölker M., Schüssler M., Weisshaar E., 1989, in Solar and Stellar Granulation, R.J. Rutten, G. Severino (Eds.), Kluwer, Dordrecht, p. 481

Gustafsson B., 1973, *Uppsala Astron. Obs. Ann.* 5, No. 6

Holweger H., Gehlsen M., Ruland F., 1978, A&A 70, 537

Jahn K., 1989, A&A 222, 264

Jones H.P., 1985, in Chromospheric Diagnostics and Modelling, B.W. Lites (Ed.), National Solar Obs., Sunspot, NM, p. 175

Kawakami H., 1983, , PASJ 35, 459

Keller C.U., Solanki S.K., Steiner O., Stenflo J.O., 1990, A&A 233, 583

Kopp G., Hartman P., Jaksha D., Plymate C., Rabin D., Wagner J., 1992, in Cool Stars, Stellar Systems and the Sun, VII, J. Bookbinder, M. Giampapa (Eds.), Astron. Soc. Pacific Conf. Series, in press

Landi Degl'Innocenti E., 1979, Sol. Phys. 63, 237

Lites B.W., Skumanich A., 1990, ApJ 348, 747

Livingston W., 1991, in Solar Polarimetry, L. November (Ed.), National Solar Obs., Sunspot, NM, p. 356

Livingston W., Wallace L., 1991, *An Atlas of the Solar Spectrum in the Infrared from 1850 to 9000 cm^{-1} (1.1 to 5.4 μm)*, NSO Technical Report # 91-001, National Solar Obs., Tucson, AZ

Makita M., 1979, PASJ 31, 575

Maltby P., Avrett E.H., Carlsson M., Kjeldseth-Moe O., Kurucz R.L., Loeser R., 1986, ApJ 306, 284

McPherson M.R., Lin H., Kuhn J.R., 1992, Sol. Phys. in press

Moore R.L., 1981, ApJ 249, 390

350

Moore R.L., Rabin D., 1985, ARA& A 23, 239

Murphy G.A., 1990, NCAR Cooperative Thesis No. 124

Murphy G.A., Rees D.E., 1990, *Operation of the Stokes Profile Synthesis Routine*, NCAR Technical Note, NCAR/TN-348+IA

Obridko V.N., Staude J., 1988, A& A 189, 232

Osherovich V.A., 1982, Sol. Phys. 77 63

Osherovich V.A., Garcia H.A., 1989, ApJ 336, 468

Pizzo V.J., 1986, ApJ 302, 785

Press W.H., Flannery B.P., Teukolsky S.A., Vetterling W.T., 1990, *Numerical Recipes. The Art of Scientific Computing*, Cambridge University Press, Cambridge

Rees D.E., Murphy G.A., Durrant C.J., 1989, ApJ 339, 1093

Rüedi I., Solanki S.K., Livingston W., Stenflo J.O., 1992a, A& A 263, 323 (Paper III)

Rüedi I., Solanki S.K., Rabin D., 1992b, A&A in press (Paper IV)

Schüssler M., 1986, in Small Scale Magnetic Flux Concentrations in the Solar Photosphere, W. Deinzer, M. Knölker, H.H. Voigt (Eds.), Vandenhoeck & Ruprecht, Göttingen, p. 103

Schüssler M., 1990, in Solar Photosphere: Structure, Convection and Magnetic Fields, J.O. Stenflo (Ed.), Kluwer, Dordrecht, IAU Symp. 138, 161

Skumanich A., Lites B.W., 1987, ApJ 322, 473

Solanki S.K., Schmidt H.U., 1992, A&A, submitted

Solanki S.K., Keller C., Stenflo J.O., 1987, A& A 188, 183

Solanki S.K., Rüedi I., Livingston W., 1992a, A&A 263, 312 (Paper II)

Solanki S.K., Walther U., Livingston W., 1992b, A& A to be submitted (Paper VI)

Stenflo J.O., 1985, in Measurements of Solar Vector Magnetic Fields, M.J. Hagyard (Ed.), NASA Conf. Publ. 2374, p. 263

Thomas J.H., Weiss N., 1992, *Theory of Sunspots*, Proc. NATO Advances Studies workshop, Cambridge, Sept. 1991, in press

Wallace L., Livingston W., 1992, *An Atlas of a Dark Sunspot Umbral Spectrum from 1970 to 8640 cm^{-1} (1.16 to 5.1 μm)*, NSO Techn. Rep. 92–001, National Solar Obs., Tucson, AZ

Wittmann A.D., 1974, Sol. Phys. 36, 29